

Validating gallium nitride growth kinetics using a precursor delivery showerhead as a novel chemical reactor

Rinku P. Parikh^a, Raymond A. Adomaitis^{a,*}, Michael E. Aumer^b, Deborah P. Partlow^b,
Darren B. Thomson^b, Gary W. Rubloff^c

^aDepartment of Chemical and Biomolecular Engineering and Institute for Systems Research, University of Maryland,
2267 A.V. Williams Building, College Park, MD 20742, USA

^bAdvanced Materials and Semiconductor Device Technology Center, Northrop Grumman Electronic Systems, Baltimore, MD 21203, USA

^cDepartment of Materials Science and Engineering and Institute for Systems Research, University of Maryland, College Park, MD 20742, USA

Received 7 April 2006; received in revised form 17 July 2006; accepted 20 July 2006

Communicated by R.M. Biefeld

Abstract

Accurate prediction of epitaxial thin film properties requires complete knowledge of the chemical reaction kinetics that occurs in the gas phase and at the deposition surface. The choice of reactor operating conditions and physical designs has a significant influence on the selectivity among different reaction pathways, as is the case in GaN where two competing reaction pathways exist. The extent to which each pathway participates in the total deposition scheme is a function of reactor geometry, operating conditions, and the degree of precursor mixing as determined by the design of gas delivery systems. A detailed chemistry model is developed in this paper to study the interplay between the transport of reactants, adduct formation chemistry, and deposition kinetics within a MOVPE reactor showerhead system. This paper will demonstrate both qualitative and quantitative validation of the chemistry model to showerhead deposition experiments.

© 2006 Elsevier B.V. All rights reserved.

Keywords: A1. Distributed parameter systems; A3. Metalorganic vapor phase epitaxy; B1. Gallium nitride

1. Introduction

Gallium nitride together with AlN and InN are considered key III–V compound semiconductors for developing advanced electronic and optoelectronic devices. Metalorganic vapor phase epitaxy (MOVPE) has emerged as the principal technique of choice for growth of single-crystalline layers of GaN [1]. However, understanding the mechanisms governing epitaxial growth of GaN is made complicated by an intricate network of chemical reactions between the commonly used precursors trimethylgallium ((CH₃)₃Ga) and ammonia (NH₃). Several research groups have conducted experimental and theoretical kinetic studies in an effort to construct reaction mechanisms describing GaN growth. A majority of these reaction

mechanisms describe GaN growth by means of two competing reaction routes: adduct formation and thermal decomposition (Fig. 1).

The adduct formation route is characterized by a spontaneous gas phase reaction between trimethylgallium ((CH₃)₃Ga) and ammonia (NH₃), to form stable Lewis acid–Lewis base adducts [2,3]. Upon formation, the adduct molecule can either revert to TMG and NH₃ or undergo a methane elimination step leaving dimethylgallium amide, (CH₃)₂Ga:NH₂ in the gas-phase. What happens after methane elimination is not fully understood. Oligomerization of the dimethylgallium amide, (CH₃)₂Ga:NH₂, to form a six member ring compound, [(CH₃)₂Ga:NH₂]₃, is frequently included as a major pathway in the mechanisms proposed in the literature [1,4–8]. The final step in the adduct formation route is unidentified, but generally is represented by the breakdown of the trimer species into low molecular weight products and large amounts of

*Corresponding author. Tel.: +1 301 405 2969; fax: +1 301 314 9920.

E-mail address: adomaiti@umd.edu (R.A. Adomaitis).

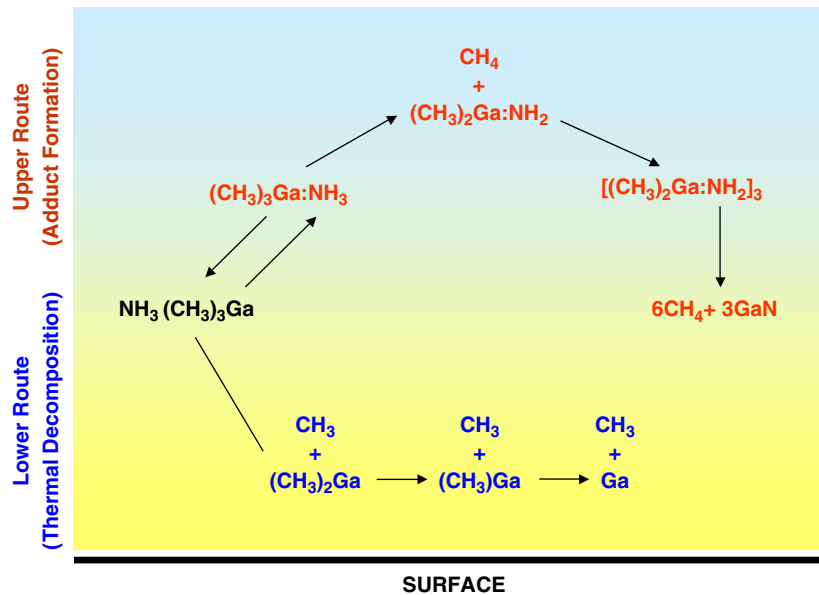


Fig. 1. Gallium nitride gas phase chemical reaction pathway consisting of upper (adduct formation) and lower (thermal decomposition) routes.

methane. Due to a limited amount of information on these low molecular weight products, their physical properties are taken to be that of GaN in this paper.

Unlike the adduct formation route, the thermal decomposition route is relatively well understood. The decomposition pathway is characterized by three sequential, first-order reactions. The first reaction is the breakdown of TMG to dimethyl-gallium (DMG) and a methyl radical. In the same fashion, two more methyl radicals are formed as DMG decomposes to monomethyl-gallium (MMG) which eventually gives elemental gallium (Ga). These reactions produce a total of three methyl radicals per TMG molecule; the kinetic data associated with this decomposition pathway is routinely included in kinetic models describing growth of GaN by numerous research groups [1,5,6]. An overview of both adduct formation and thermal decomposition routes is found elsewhere [9].

The extent of gas-phase reactions can be controlled through the design of gas delivery systems which range from those resulting in complete mixing to minimal or no mixing of the precursors before being fed to the reactor chamber. It should be noted that for designs that suppress reactions in the gas delivery system, complete mixing of the precursors must take place close to the wafer surface to facilitate uniform film thickness [1]. Accordingly, optimization studies geared towards understanding the relationship between reactor geometry, operating conditions, and deposition kinetics have been performed by others [4,10–12]. Studies such as these give insight into how reactor design elements should be modified to best achieve high-quality thin films of GaN with a spatially uniform thickness.

This paper studies the interplay between the transport of reactants, adduct formation chemistry, and deposition kinetics within a MOVPE reactor showerhead system.

The reactor consists of a cooled-wall horizontal chamber with a showerhead above a single wafer resting on a heated susceptor (Fig. 2). In this design, reactant precursors are completely mixed before being fed to the showerhead allowing us to study one extreme case for the range of gas delivery system designs discussed above. Holes are arranged in a series of concentric rings in the showerhead and are drilled through the lower quartz plate. The transparency of the showerhead provides a unique design feature which enables us to make the connection between reactor design and chemical kinetics as concrete as possible: after each growth run, the showerhead is removed from the reactor and significant deposition is observed (Fig. 3). More importantly, the deposition pattern is distinct in that there exists two physically different regions: a central region with little or no deposits and an annular region containing large amounts of deposits.

A detailed transport-reaction model is developed in this paper and applied to the showerhead portion of this reactor configuration. The model attempts to capture the deposition process inside the showerhead in both a qualitative (spatial distribution of deposition pattern) and quantitative (weight measurements) fashion. The paper is organized in the following manner—a brief overview of the heat and transport model, and a discussion of the kinetic model are presented in Sections 2.1 and 2.2, respectively. In Section 3, comparison between experimental results and model predictions is presented.

2. Showerhead model development

2.1. Heat transfer and species transport model

Expanding on some of the ideas for showerhead modeling presented in Ref. [13], a physically based model

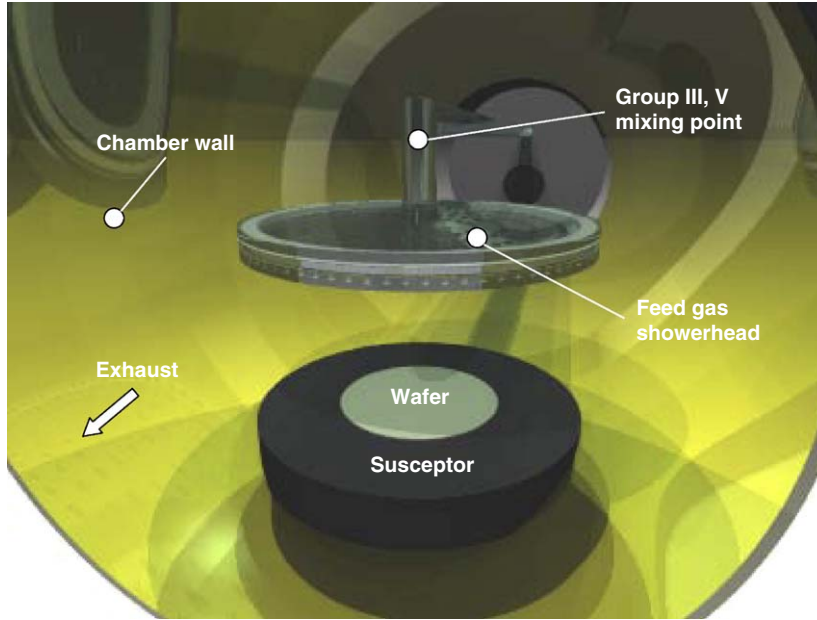


Fig. 2. Single wafer MOVPE reactor showerhead system.



Fig. 3. Showerhead deposition pattern: before growth run (left) and after growth run (right).

describing heat transfer and gas transport through the showerhead was developed by Hoffman and Adomaitis [14]. Their model was constructed from simplified descriptions of gas flow and heating through each component in the showerhead. The model predicts gas velocity (v), gas density (ρ), gas temperature (T_{gas}), and pressure (P) at radial positions inside the showerhead. A complete description of the showerhead heat and transport model is found in the cited work [14]. However, because results obtained from their model are subsequently used as inputs into the kinetic model developed in this paper, key aspects of the showerhead heat and transport model are presented in this section.

A cross-sectional view of the showerhead configuration is shown in Fig. 4. Notation for some showerhead design parameters and simulation variables are denoted as

hole ring radii : R_1, \dots, R_M ,

gas radial velocity inside showerhead : u_1, \dots, u_{2M-1} ,

reactant gas velocity through holes : v_1, \dots, v_M ,

and showerhead gas pressure : P_1, \dots, P_{2M-1} .

where $m = 1, 2, \dots, M$ ($m = 1$ always refers to the showerhead center, whether or not a center hole is used).

2.1.1. Radial flow momentum and mass balances

A momentum balance for the radial component of the inter-plate gas velocity field can be written as

$$\frac{\rho}{2} \frac{\partial v_r^2}{\partial r} = -\frac{\partial P}{\partial r} + \mu \frac{\partial}{\partial r} \frac{1}{r} \frac{\partial}{\partial r} r v_r + \mu \frac{\partial^2 v_r}{\partial z^2} \quad (1)$$

assuming ρ and μ are constant within each segment region.¹ Under the assumption of fully developed laminar

¹Note that the physical properties will vary from segment region to segment region depending on the region's temperature and mean pressure.

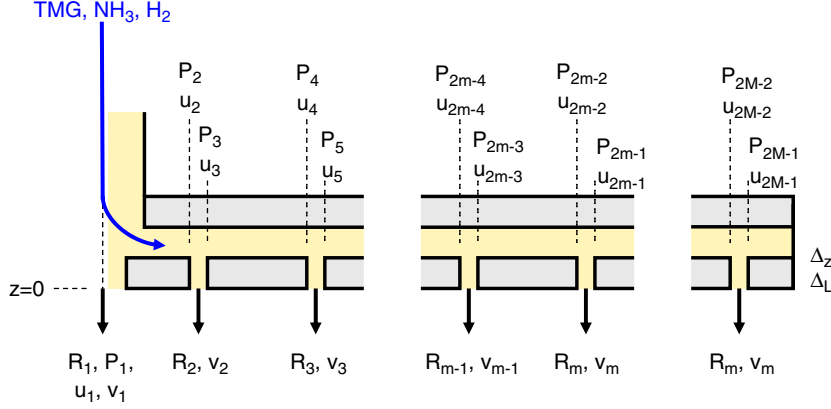


Fig. 4. A cross-sectional view of the showerhead configuration and notation for the design parameters and simulation variables.

gas flow in the showerhead,² the radial component of gas velocity v_r can be written as

$$v_r = v_r^{\max} \left[\left(\frac{\Delta z}{2} \right)^2 - z^2 \right] \left(\frac{4}{\Delta z^2} \right). \quad (2)$$

Defining u to be the mean over z , we find

$$u(r) = \frac{2}{3} v_r^{\max}. \quad (3)$$

In between the rings of holes,³ the continuity equation gives

$$\frac{d}{dr} r u = 0. \quad (4)$$

Therefore, if the velocity profile at the entrance to each inter-ring segment is $v_{r,m}^{\text{in}}(z)$, the velocity profile within this segment can be written as

$$v_r(r, z) = \frac{v_{r,m}^{\text{in}}(z) R_{m-1}}{r}. \quad (5)$$

Constant gas density in between the rings of holes is assumed in the derivation of the continuity equation for the model developed in this section. However, it should be noted that a small modification to the constant density continuity equation (4) is used for the kinetic model developed in Section 2.2 in order to maintain accurate species material balances.

Substituting Eq. (3) into Eq. (2) and comparing the result to Eq. (5), we see that

$$v_r = \frac{3}{2} u_{2m-3} \left[\left(\frac{\Delta z}{2} \right)^2 - z^2 \right] \left(\frac{4}{\Delta z^2} \right) \left(\frac{R_{m-1}}{r} \right). \quad (6)$$

Eq. (6) now is differentiated twice with respect to z and the result is substituted into the last term of Eq. (1); the continuity equation (4) eliminates the second-to-last term

of Eq. (1) giving

$$\frac{\rho}{2} \frac{dv_r^2}{dr} = -\frac{dP}{dr} - \frac{12\mu u_{2m-3}}{\Delta z^2} \left(\frac{R_{m-1}}{r} \right) + g(u_{2m-3}), \quad (7)$$

where the nonlinear term $g(u)$ accounts for deviations in the true contribution of frictional losses due to non-fully developed flow and other effects. Because $g(u) \rightarrow 0$ as $u \rightarrow 0$, linearizing this unknown function and incorporating it in Ref. (7) gives

$$\frac{\rho}{2} \frac{dv_r^2}{dr} = -\frac{dP}{dr} - \frac{12\mu k_f u_{2m-3}}{\Delta z^2} \left(\frac{R_{m-1}}{r} \right), \quad (8)$$

where the friction factor $k_f > 0$ will be determined from across-wafer uniformity measurements [14].

Averaging Eq. (8) over z and assuming the pressure P is a weak function of z gives

$$\frac{3\rho}{5} \frac{du^2}{dr} = -\frac{dP}{dr} - \frac{12\mu k_f u_{2m-3}}{\Delta z^2} \left(\frac{R_{m-1}}{r} \right). \quad (9)$$

Integrating Eq. (9) over one of the regions between consecutive hole rings gives

$$\begin{aligned} \frac{3\rho}{5} (u_{2m-2}^2 - u_{2m-3}^2) &= -P_{2m-2} + P_{2m-3} \\ &\quad - \frac{12k_f \mu u_{2m-3} R_{m-1}}{\Delta z^2} \ln \frac{R_m}{R_{m-1}}, \quad m = 3, 4, \dots, M. \end{aligned} \quad (10)$$

A momentum balance (after Ref. [15]) at each hole ring junction point gives

$$P_{2m-2} - P_{2m-1} = k_p \rho (u_{2m-1}^2 - u_{2m-2}^2), \quad m = 2, 3, \dots, M, \quad (11)$$

where a (positive) pressure jump occurs at each hole ring due to the drop in radial velocity resulting from gas flowing out of the ring of showerhead holes. The correction factor $0 \leq k_p \leq 1$ is discussed in Ref. [15] and accounts for any radial velocity component of the flow leaving the control volume through the showerhead holes.

²Calculation of the Reynolds number for the gas flow between two parallel plates for nominal operating condition shows this is a valid assumption.

³We assume $R_m - R_{m-1} \gg R_h$ in the derivation of all modeling equations.

2.1.2. Flow through the showerhead holes

Each hole in the lower showerhead plate forms a cylinder with radius R_h and length Δ_L . The coordinate system for each hole consists of the local radial position r' (i.e., $r' = 0$ at each hole centerline) and global axial direction z . A momentum balance for the reactant gas passing through a showerhead hole gives

$$\frac{\rho}{2} \frac{\partial v_z^2}{\partial z} = -\frac{\partial P}{\partial z} - \mu \frac{1}{r'} \frac{\partial}{\partial r'} \left(r' \frac{\partial v_z}{\partial r'} \right).$$

If v_m is the mean velocity of the gas passing through each showerhead hole and accounting for any deviations from fully developed flow in the same manner as Eq. (7), the momentum balance equation can be reduced to the following simplified form:

$$\frac{2\rho}{3} v_m^2 + \frac{8k_s \mu v_m \Delta_L}{R_h^2} = \frac{P_{2m-2} + P_{2m-1}}{2} - P_c, \quad m = 2, 3, \dots, M \quad (12)$$

(compare this to Eq. (7) of Ref. [13]). We note this equation uses the mean of the pressure difference across each hole row (11); the equation describing the gas velocity through the center hole (v_1) is

$$\frac{2\rho}{3} v_1^2 + \frac{8k_s \mu v_1 \Delta_L}{R_h^2} = \frac{P_1 + 2P_{ft}}{3} - P_c \quad (13)$$

with

$$P_{ft} = P_1 - \frac{3\rho}{5} u_{ft}^2, \quad u_{ft} = u_2 \frac{r_2}{R_{ft}}. \quad (14)$$

In these equations, P_{ft} , u_{ft} , and R_{ft} represent the feed tube pressure, velocity, and radius, respectively.

2.1.3. Continuity equations

A material balance over the center-most region of the showerhead gives

$$Q\rho_1 - 2\pi R_2 \Delta z u_2 \rho_1 = \pi N_1 R_h^2 v_1 \rho_1 \quad (15)$$

and a material balance at each showerhead ring junction gives

$$2R_m \Delta z (u_{2m-2} \rho_{m-1} - u_{2m-1} \rho_m) = N_m R_h^2 v_m \rho_m, \quad m = 2, 3, \dots, M. \quad (16)$$

Here, Q represents the total volumetric flow into the showerhead and N_m the number of holes in each ring. Finally, the continuity equation between each ring relates the radial velocity value at the downstream edge of one hole ring to the velocity at the leading edge of the next ring:

$$R_m u_{2m-2} = R_{m-1} u_{2m-3}, \quad m = 3, 4, \dots, M. \quad (17)$$

Symmetry at $r = 0$ and no radial flow at $r = R_{sh}$ (R_{sh} corresponds to the radius of the showerhead) require

$$u_1 = 0, \quad u_{2M-1} = 0 \quad (18)$$

and the centerline pressure P_1 is approximated as the sum of the pressure drop required to accelerate the gas to the radial velocity u_{ft} and the pressure difference found using

Eq. (10) evaluated over $R_{ft} \leq r \leq R_2$:

$$\frac{3\rho}{5} u_2^2 = -P_2 + P_1 - \frac{12k_f \mu u_{ft} R_{ft}}{\Delta z^2} \ln \frac{R_2}{R_{ft}}, \quad (19)$$

where u_{ft} was defined in Eq. (14). Recall that the pressure P_1 includes the influence of the $(3\rho/5)u_{ft}^2$ term contained in its definition (14).

2.1.4. Showerhead temperature model

The temperature distribution for the top showerhead plate $T_{top}(r)$, the bottom showerhead plate $T_{bot}(r)$, and the reactant gas flowing in between them $T_{gas}(r)$ is computed from an energy balance that takes into account three modes of heat transfer: radiation, conduction, and sensible heat changes due to flow and heating of the reactants inside the showerhead (Fig. 5). Radiative heat transfer occurs between the following reactor elements: heated susceptor (wafer) and showerhead bottom and top plates; showerhead top and the reactor liner walls; and top and bottom plates themselves. Conduction of heat occurs between the following reactor elements: showerhead and susceptor; showerhead top and liner walls; and reactant gas and showerhead top and bottom plates. Based on simulation studies of the heat transfer model, an accurate representation of the radiative heat transfer between the showerhead top plate and the susceptor as a result of reflection off the liner tube reflective gold coating (q_{rrw} in Fig. 5) is essential in predicting accurate temperature distributions. An important parameter in this energy balance is γ , which represents the percentage of the liner surface that is covered with a gold coating. The value of γ is set between the 0 and 1, where $\gamma = 1$ corresponds to a fully coated (highly reflective) liner.

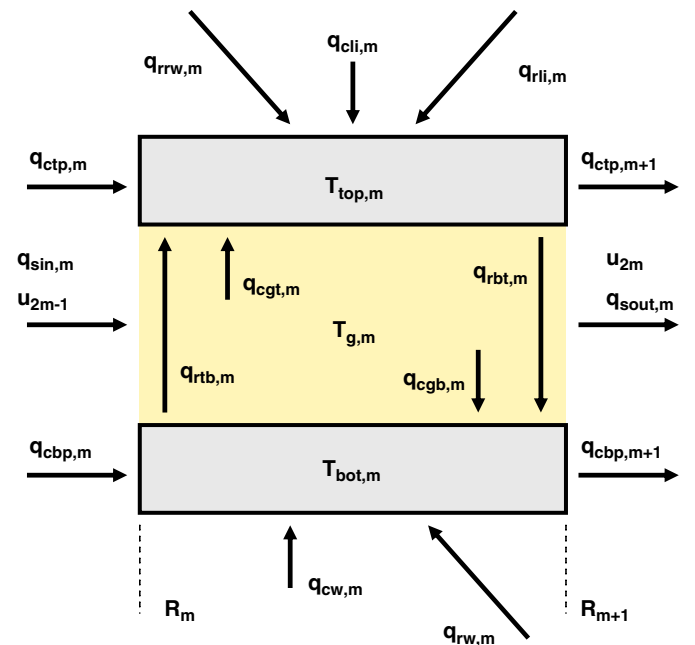


Fig. 5. A cross-sectional view of a showerhead annular segment, showing all relevant heat transfer terms.

The temperature distribution of the showerhead plates and reactant gas is approximated by a piece-wise continuous and locally constant function. The modeling equations to be solved consist of a large set of nonlinear algebraic equations: the equations describe the spatially discretized showerhead gas energy balance, the showerhead top and bottom plate energy balances, and the showerhead gas momentum balances and continuity equations.

Results for gas velocity, pressure, gas temperature, and top and bottom showerhead plate temperatures are shown in Fig. 6 for a nominal set of operating conditions: pressure = 200 Torr; susceptor temperature = 1308 K; total flow ($\text{NH}_3 + \text{H}_2$) = 20 slm. It is apparent in Fig. 6 that the temperature of both the top and bottom showerhead plates are hot relative to the gas temperature in the central region of the showerhead. This is a result of the cool gas feed and radiative heating of the showerhead. As the gas flows outward, the gas temperature increases and reaches a level somewhere between the two plate temperatures. The result for gas velocity and internal showerhead pressure are also shown in Fig. 6. A decrease in gas velocity is observed due to the cylindrical geometry of the inter-plate showerhead space. The circles denote hole ring locations that give rise to jumps in velocity and pressure observed in the figure. Note that the jump in velocity is a function of the change in gas temperature and flow out the hole ring, and

so maybe positive or negative. The following section combines these results with a detailed kinetic model to provide spatial chemical species distributions within the showerhead.

2.2. Kinetic model

A detailed one-dimensional showerhead reaction model is developed in this section. Rate parameters for all gas phase reactions included in the model are given in Table 1. The rate of G4 is assumed to be collision limited and is derived from the kinetic theory of gases [16]. The bimolecular collision rate expression is given by

$$k = \pi \sigma_{AB}^2 \left(\frac{8k_B T}{\pi \mu} \right)^{0.5}, \quad (20)$$

where μ is the reduced mass, T the absolute temperature in the gas phase, k_B the Boltzmann's constant and σ_{AB} is the mean collision diameter of molecule A and B given by

$$\sigma_{AB} = \frac{1}{2}(\sigma_A + \sigma_B). \quad (21)$$

In this case, σ_A and σ_B represent the individual collision diameters of TMG and NH_3 having values of 5.47 Å [17] and 2.92 Å [18], respectively. The activation energy for the forward reaction is 0 kcal/mole indicating adduct formation is spontaneous. Similarly, the rate of trimer formation

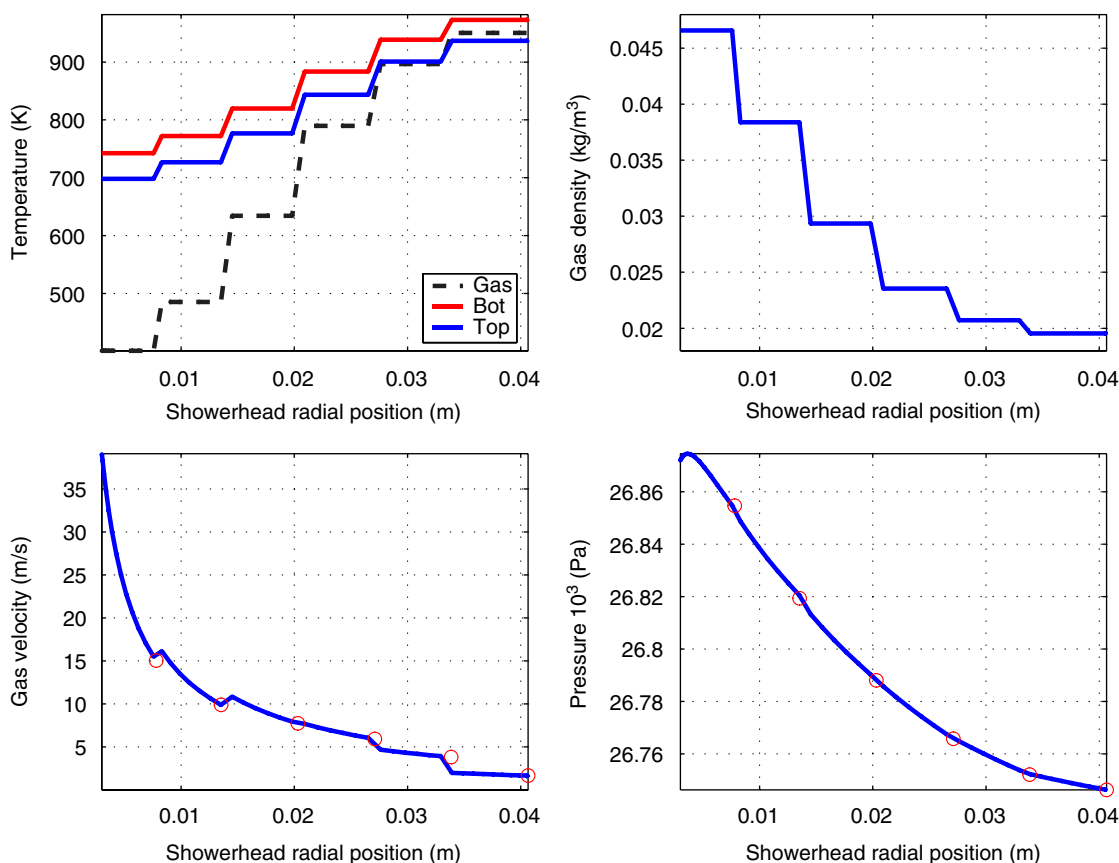


Fig. 6. Showerhead gas temperature along with top and bottom plate temperatures (upper left); gas density (upper right); gas velocity (lower left); and pressure (lower right) for nominal set of operating conditions: pressure = 200 Torr; susceptor temperature = 1308 K; total flow ($\text{NH}_3 + \text{H}_2$) = 20 slm.

Table 1
Representative gas-phase reaction scheme for MOVPE of GaN from trimethylgallium and ammonia

Rxn. no	Reactions	k_0	E_a	n	Ref.
G1	$(\text{CH}_3)_3\text{Ga} \rightarrow (\text{CH}_3)_2\text{Ga} + \text{CH}_3$	3.5×10^{15}	59.5	0.0	[19]
G2	$(\text{CH}_3)_2\text{Ga} \rightarrow (\text{CH}_3)\text{Ga} + \text{CH}_3$	8.7×10^7	35.4	0.0	[19]
G3	$(\text{CH}_3)\text{Ga} \rightarrow \text{Ga} + \text{CH}_3$	1.0×10^{16}	77.5	0.0	[19]
G4	$(\text{CH}_3)_3\text{Ga} + \text{NH}_3 \rightarrow (\text{CH}_3)_3\text{Ga} : \text{NH}_3$	coll. (20)	0.0	0.0	[1]
G5	$(\text{CH}_3)_3\text{Ga} : \text{NH}_3 \rightarrow (\text{CH}_3)_3\text{Ga} + \text{NH}_3$	9.5×10^9	18.5	0.0	[6]
G6	$(\text{CH}_3)_3\text{Ga} : \text{NH}_3 \rightarrow (\text{CH}_3)_2\text{Ga} : \text{NH}_2 + \text{CH}_4$	1.0×10^{14}	49.0	0.0	[1]
G7	$3[(\text{CH}_3)_2\text{Ga} : \text{NH}_2] \rightarrow [(\text{CH}_3)_2\text{Ga} : \text{NH}_2]_3$	coll. (22)	0.0	0.0	[1]
G8	$[(\text{CH}_3)_2\text{Ga} : \text{NH}_2]_3 \rightarrow 3\text{GaN} + 6\text{CH}_4$	4.0×10^{15}	60.0	0.0	[6]

Activation energies are in (kcal/mole) and pre-exponentials are in $(\text{cm}^3/\text{mole})^{\alpha-1} \text{s}^{-1}$, where α is the order of reaction. Rate constants are given by $k = k_0 T^m \exp(-E_a/RT)$.

represented by reaction G7 also is expressed as being collision limited and is governed by the probability of a three-body collision between three dimethylgallium amide molecules. The intermolecular collision rate is given by

$$k = \pi \sigma_A^5 \left(\frac{8k_B T}{\pi m_A} \right)^{0.5}, \quad (22)$$

where the collision diameter, σ_A , of $(\text{CH}_3)_2\text{Ga}:\text{NH}_2$ is calculated to be 5.39 \AA based on group contribution methods [18] and m_A is the mass of $(\text{CH}_3)_2\text{Ga}:\text{NH}_2$.

Up to this point, we have only discussed gas phase reactions that can occur between TMG and ammonia. Gas surface reactions which describe the interaction of gas phase species with a reactive surface also are included in this model and are shown in Table 2. The rate of all adsorption reactions is assumed to be controlled by two factors: the rate of collision of gas-phase species with the surface and the fraction of incident molecules which become adsorbed. Therefore, the adsorption rate of the i th species, R_i^S , can be expressed as the product of the flux of species i , F_i , and its sticking probability, S_i .

$$R_i^S = F_i \cdot S_i. \quad (23)$$

The sticking probability lies in the range $0 \leq S_i \leq 1$, where the two extremes correspond to no molecules being adsorbed or complete adsorption of all incident molecules, respectively. The flux, F_i , is derived from the kinetic theory of gases and governed by the Hertz–Knudsen equation [16]:

$$F_i = \frac{P}{(2\pi m_i R_{\text{gas}} T)^{0.5}} \cdot x_i \quad (24)$$

Here F_i represents the flux of species i (mole/area/time), P the total pressure, m_i is the molecular weight of species i , R_{gas} is the ideal gas constant, T is the temperature, and x_i corresponds to the mole fraction of species i in the gas phase above the surface. In our model, we assume that the activation energies are all set to 0 kcal/mole. The sum of the fluxes of TMG, DMG, MMG, Ga, DMG: NH_2 , and GaN are assumed to govern the growth rate, and accordingly, sticking probabilities for those species are set equal to unity

Table 2
Representative surface-phase reaction scheme for gallium nitride growth

Rxn. no	Reactions	k_0	E_a
S1	$(\text{CH}_3)_3\text{Ga} + \text{S} \rightarrow \text{Ga}(\text{s}) + 3\text{CH}_3$	$S_1 = 1$	0.0
S2	$(\text{CH}_3)_2\text{Ga} + \text{S} \rightarrow \text{Ga}(\text{s}) + 2\text{CH}_3$	$S_2 = 1$	0.0
S3	$(\text{CH}_3)\text{Ga} + \text{S} \rightarrow \text{Ga}(\text{s}) + \text{CH}_3$	$S_3 = 1$	0.0
S4	$\text{Ga} + \text{S} \rightarrow \text{Ga}(\text{s})$	$S_4 = 1$	0.0
S5	$(\text{CH}_3)_3\text{Ga} : \text{NH}_3 + 2\text{S} \rightarrow \text{GaN}(\text{s}) + 3\text{CH}_4$	$S_5 = 0$	0.0
S6	$(\text{CH}_3)_2\text{Ga} : \text{NH}_2 + 2\text{S} \rightarrow \text{GaN}(\text{s}) + 2\text{CH}_4$	$S_6 = 1$	0.0
S7	$[(\text{CH}_3)_2\text{Ga} : \text{NH}_2]_3 + 6\text{S} \rightarrow 3\text{GaN}(\text{s}) + 6\text{CH}_4$	$S_7 = 0$	0.0
S8	$\text{GaN} + \text{S} \rightarrow \text{GaN}(\text{s})$	$S_8 = 1$	0.0

S represents a free surface site.

while sticking probabilities for the remaining species are set to zero.

A material balance is written for each chemical species

$$\frac{1}{R} \frac{d}{dR} (cx_i uR) = R_i^G + \frac{2R_i^S}{\Delta Z/2}. \quad (25)$$

Here c is the total concentration of the gas ($c = P/R_{\text{gas}}/T$ for an ideal gas, P is the total reactor pressure, and R_{gas} corresponds to the ideal gas constant), x_i is the mole fraction of the i th species, ΔZ the distance between the top and bottom showerhead plates, R_i^G the rate of generation of species i per unit volume due to gas phase reactions and R_i^S the rate of generation of species i per unit area due to surface phase reactions. The quantity $2R_i^S$ results from the assumption that deposition occurs on both the bottom and top showerhead plates.

Eq. (25) is denoted for each annular segment in the showerhead (region between hole rings). The temperature profile within each annular segment is assumed to be a linear fit between the trailing and leading segment gas temperatures, derived from the stair-like function shown in Fig. 6. The velocity profile within each annular segment then is computed through the equation of continuity

$$\frac{d}{dR} (u\rho R) = 0. \quad (26)$$

It should be noted that the equation of continuity used for the transport-reaction model developed in this section is slightly different than the one used in Eq. (4) in order to maintain accurate chemical species material balances. In addition, inlet mole fractions for all chemical species are set equal to the corresponding outlet mole fractions from the previous segment.

Species mole fraction distributions of each chemical species are shown in Fig. 7 based on the nominal set of operating conditions: pressure = 200 Torr; susceptor temperature = 1308 K; total flow ($\text{NH}_3 + \text{H}_2$) = 20 slm. The results indicate that the adduct molecule, TMG:NH_3 , is the major gallium-containing species present until a radial position of 2 cm. Thereafter, as the gas temperature increases, other reactions become significant producing an array of gallium-containing species.

The deposition rate profile is a function of the gas phase mole fraction of TMG, DMG, MMG, Ga, DMG:NH_2 , and GaN and is represented by

$$\Delta(R) = \sum_{i=1}^N R_i^S \cdot x_i. \quad (27)$$

The deposition pattern predicted from the model corresponding to nominal reactor operating conditions is

compared to experimental observations in Fig. 8. The model accurately captures the deposition pattern left in the showerhead after one run and now will be used to explore the interaction between the transport of reactants, adduct formation chemistry, and deposition kinetics. All simulations were done using the quadrature-based weighted residual method techniques of Adomaitis [20].

3. Experimental and model validation

3.1. Experimental procedure

The experimental procedure was conducted in such a way to allow for both qualitative and quantitative model validation. Before starting each growth run, the showerhead was placed onto a scale to record its *pre-growth* weight. Typical growth times for GaN were 45–60 min. Upon completion of the growth run, the showerhead was removed from the reactor and again placed on the scale to record its *post-growth* weight to determine the change in showerhead weight attributable to deposition incurred during the growth run. Additionally, a picture of the showerhead deposition pattern was taken. Finally, the showerhead was placed in HF cleaning solution to remove

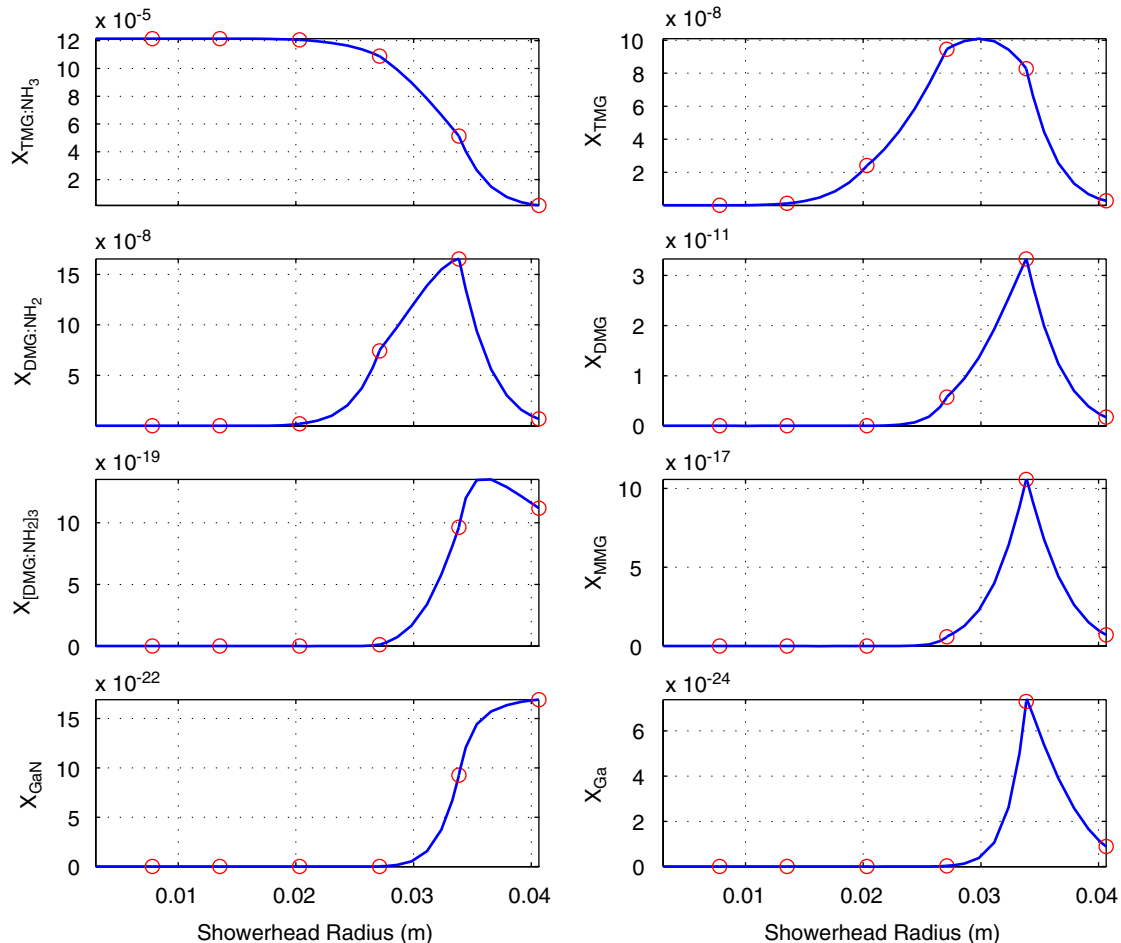


Fig. 7. Chemical species mole fraction distributions within the showerhead.

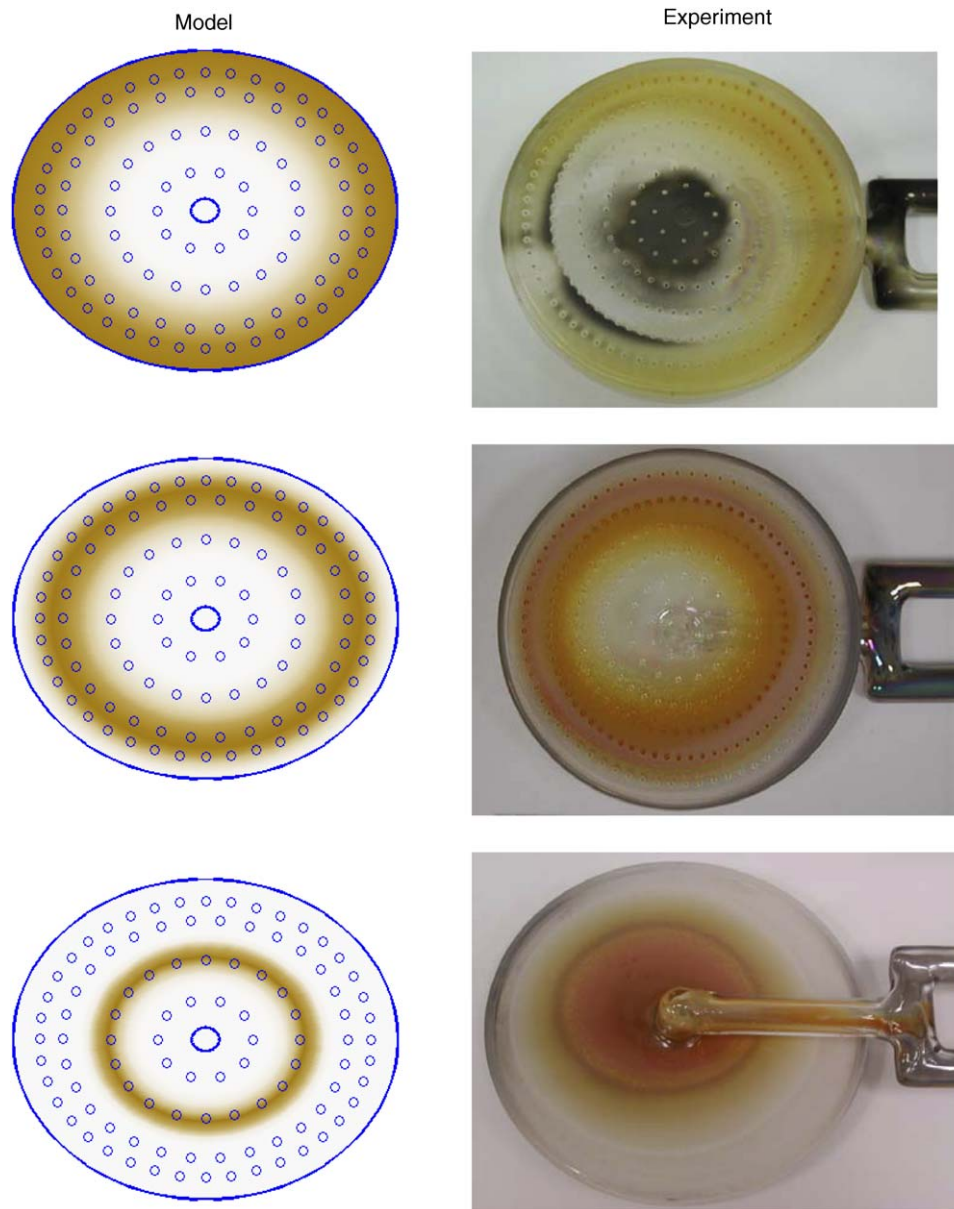


Fig. 8. Qualitative comparison between model predictions and observed showerhead deposition patterns: $T_{\text{sus}} = 1123$ K (top); $T_{\text{sus}} = 1308$ K (middle); $T_{\text{sus}} = 1523$ K (bottom). The colors for each plot are normalized with respect to the maximum deposition rate calculated for that particular showerhead.

as much of the deposits as possible. It should be noted that the normal lifetime of a showerhead is typically six or seven growth runs.

3.2. Qualitative comparison

To test the validity of the reaction-transport model it seemed most reasonable to study the effect susceptor temperature has on showerhead deposition; any change in susceptor temperature will directly influence gas temperature inside the showerhead, effectively changing the intrinsic showerhead kinetics and the corresponding deposition pattern. Experiments were performed for three different susceptor temperatures while keeping all other

growth parameters constant (reactor pressure, precursor flow rates, showerhead hole pattern, showerhead to susceptor gap, etc.). The temperature range was expanded as much as possible (within reasonable reactor limitations) in order to elucidate its effect on the observed showerhead deposition patterns. Experiments were performed for susceptor temperatures of 1123, 1308, and 1523 K. Qualitative comparison between model predictions and observed showerhead deposition patterns are shown in Fig. 8 for the three cases. The colors for each plot are normalized with respect to the maximum deposition rate calculated for that particular showerhead.

The experiments reveal significant differences in showerhead deposition patterns as susceptor temperature is

changed. The area of the central region of the showerhead where little or no deposition occurs is significantly different in the three cases. The central region of the showerhead corresponding to $T_{\text{sus}} = 1123$ K is much larger in comparison to $T_{\text{sus}} = 1308$ K. Moreover, most of the deposition for the low temperature case occurs towards the outer edge. It should be noted that the black residue are deposits on the outside of the showerhead and should be ignored in the comparison. The exact opposite is observed in the case where the $T_{\text{sus}} = 1523$ K. In this case more deposition is seen towards the showerhead center and less towards the outer edges.

In addition to the visual comparison illustrated in Fig. 8, MATLAB's image processing toolbox [21] was utilized to correlate the color pattern of the showerhead deposits in the experimental photographs to film thickness. In this approach, the showerhead images were (1) imported into MATLAB; (2) converted into a grey scale format; (3) placed onto a quadrature grid to enable accurate interpolation [20]; and (4) rotated for the purpose of averaging. Cross-sectional slices of the rotationally averaged shower-

head deposits for the three susceptor temperatures are shown in Fig. 9.

The results reveal several key points about this system. For the nominal ($T_{\text{sus}} = 1308$ K) and low temperature ($T_{\text{sus}} = 1123$ K) cases, the qualitative study results indicate that the showerhead reaction-transport model is valid. The inward movement of the deposition zone with increasing temperature is clearly seen in these results and for normal operating conditions the model does a good job of predicting experimental deposition patterns in the showerhead.

However, for the high temperature ($T_{\text{sus}} = 1523$ K) run, the results indicate that unmodeled phenomena may be at work in this system. It is reasonable to believe that at high growth temperatures, greater heating of the feed tube may take place resulting in significant gas phase reactions occurring upstream of the showerhead. To capture these phenomena, more detailed modeling of the gas delivery system upstream of the showerhead is required together with experiments to validate the heat transfer characteristics of the system upstream of the showerhead. Likewise,

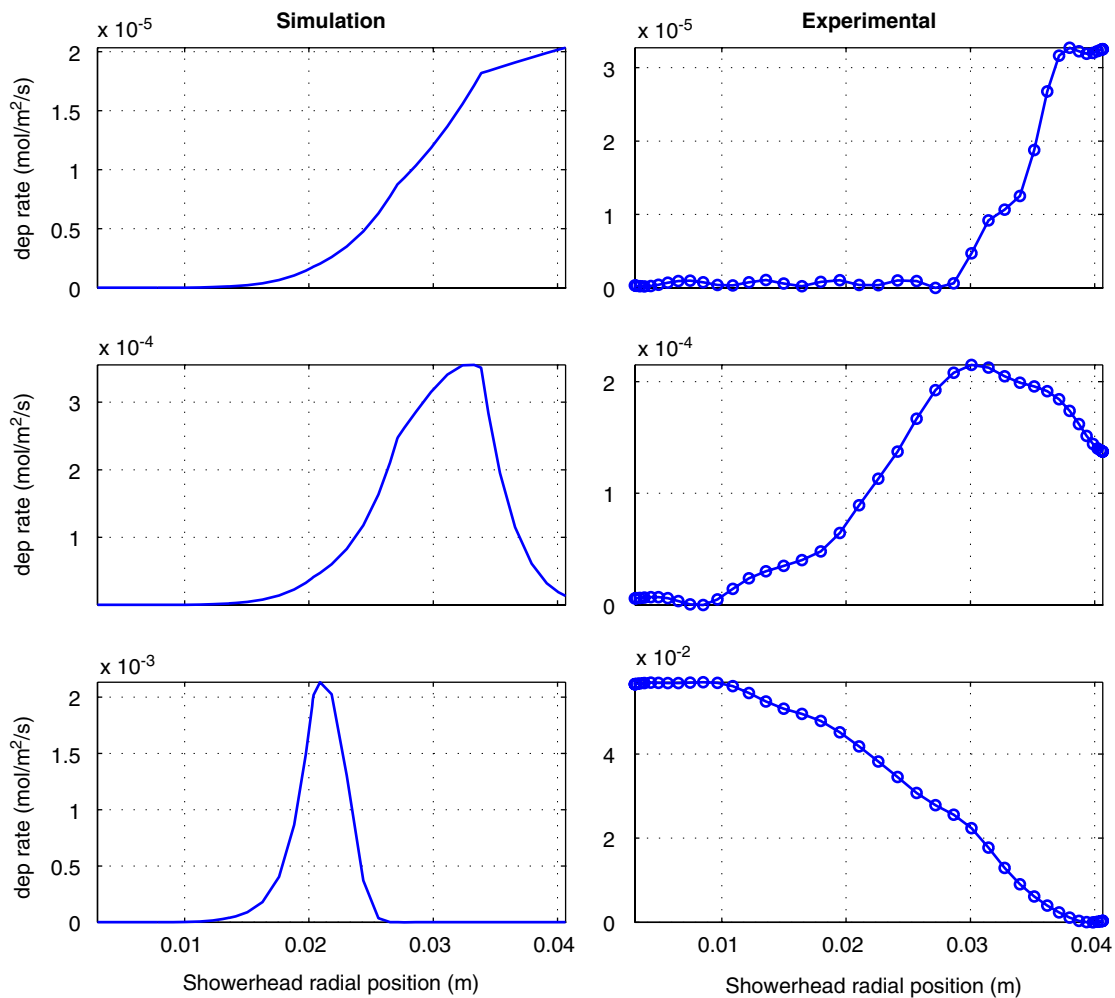


Fig. 9. Qualitative comparison between model predictions and observed showerhead deposition patterns using MATLAB image processing toolbox. $T_{\text{sus}} = 1123$ K (top); $T_{\text{sus}} = 1308$ K (middle); $T_{\text{sus}} = 1523$ K (bottom).

it is possible that additional experimental runs between the nominal temperature and high temperature regime may shed more light on the differences seen here. However, equipment availability and other resource limitations prevent such a study at this time.

3.3. Quantitative comparison

In addition to model validation based solely on qualitative means, quantitative measurements also were performed, providing further evidence on the consistency of the reaction-transport model developed in this paper. Our approach is to calculate from the model how much of the entering TMG is lost due to showerhead deposition and compare that to showerhead weight experiments. Using the model predictions, the calculation involves integration of the deposition rate profile and dividing the result by the total amount of TMG fed to the showerhead:

$$\varepsilon_M = \frac{1}{\phi} \int_{R_{in}}^{R_{sh}} \Delta(R) r dr. \quad (28)$$

Here ϕ represents the total inlet feed of TMG into the showerhead (mole/s). Based on experiments, the amount of showerhead deposition is computed by

$$\varepsilon_E = \frac{(W_{post} - W_{pre})}{\chi}. \quad (29)$$

Here χ denotes the total inlet feed of TMG into the showerhead (g) and W_{post} and W_{pre} refer to post-growth and pre-growth weights of the showerhead (g). Fig. 10 compares results between model predictions and experiments. Once again, model predictions are in good agreement to the experimental data for susceptor temperatures between 1123 and 1523 K. It should be noted that no adjustable parameters have been included in the kinetic model, and minimal parameter fitting was done with

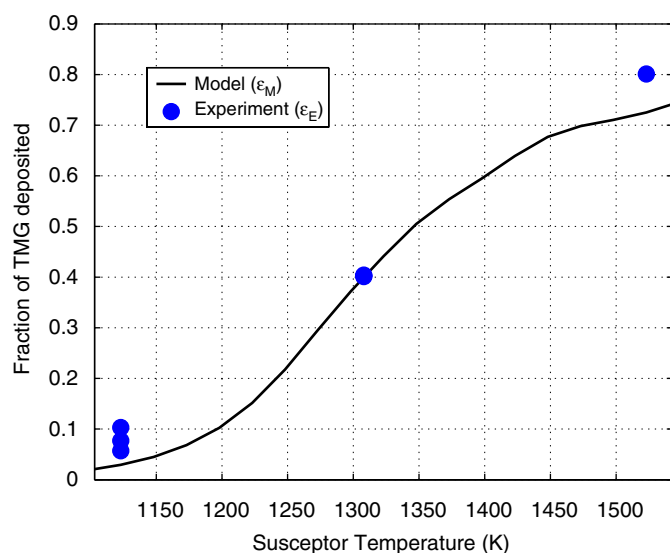


Fig. 10. Quantitative comparison between model predictions and showerhead deposition experiments: total Ga-containing species deposition.

respect to the thermal model. The only heat transfer model parameter that was fitted to the data was the liner gold coat fraction (γ). A value of $\gamma = 0.77$ was found to be the best fit to the data, a reasonable value based on the physical design of the reactor system.

3.4. Discussion

Both the showerhead design and the reactor operating conditions have a significant influence on the selectivity of reaction pathways and on the observed showerhead deposition patterns. We begin a discussion of the showerhead deposit patterns by analyzing the deposition process from a modeling perspective. Fig. 11 shows the spatial distribution of the adduct molecule, TMG:NH₃, for all three susceptor temperatures. Taking a closer look at the TMG:NH₃ profile for $T_{sus} = 1308$ K, as the precursors enter the showerhead, the temperature of the gas is cool, and the only gas-phase reaction that occurs is the spontaneous formation of the adduct species. As the adduct molecules flow radially through the showerhead they can do either of two things: exit the showerhead through the hole rings or remain in the showerhead and begin to participate in further gas phase reactions downstream. It is important to note that the adduct molecule has a sticking probability equal to zero in our model and so the adduct species does not contribute to the deposition pattern. For $T_{sus} = 1308$ K, the adduct is the major gallium-containing species until the third hole ring junction (approximately $R = 2$ cm) and, therefore, little or no deposition will occur until this location.

After the third hole ring junction, the temperature of the gas in the showerhead is sufficiently high to promote further gas phase reactions, in particular, adduct dissociation to produce TMG and NH₃ (the lower route in Fig. 1) or methane elimination to form DMG:NH₂ (upper route).

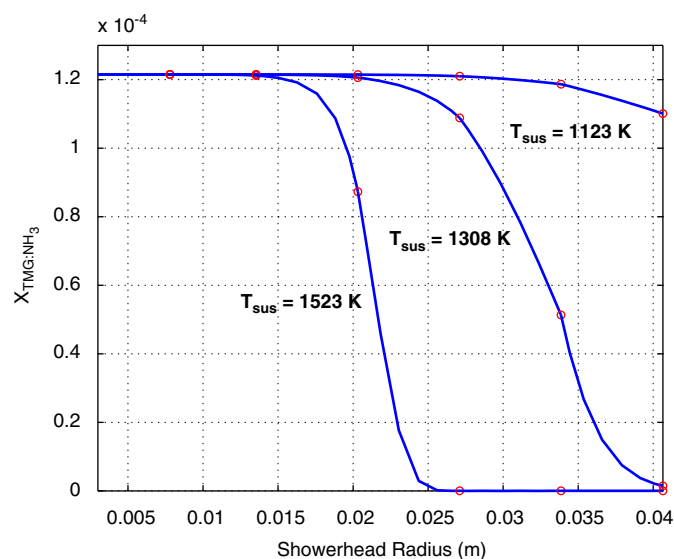


Fig. 11. Spatial distribution of adduct molecule for three susceptor temperatures. Showerhead hole rings are marked by the red circles

This is reflected by the decrease in adduct concentration starting at the third hole ring location shown in Fig. 11. Both reaction pathways are believed to occur based on our modeling work. The upper pathway leads to DMG:NH₂ which can either deposit inside the showerhead, exit the showerhead, or undergo a three-body collision to form the trimer molecule. The lower pathway of Fig. 1 produces an array of sub-alkyls, each having the potential to deposit inside the showerhead.

We believe that the direct sticking of these molecules (TMG, DMG, MMG, Ga, GaN, and DMG:NH₂) is what is responsible for the deposition observed in the showerhead. Contrary to typical epitaxial growth involving adsorption, desorption, surface migration, and surface reactions, we hypothesize that the deposition in the showerhead is a result of these molecules merely sticking to the surface. Thus, the combination of carbon, nitrogen, hydrogen, and gallium atoms present in many of the depositing species may be the basis for the dark brownish deposits seen in the showerhead.

Returning to Fig. 11, let us explain what happens to the TMG:NH₃ profiles for when the T_{sus} is reduced to 1123 K or increased to 1523 K. When the susceptor temperature is decreased to 1123 K, the gas temperature profile within the showerhead decreases. Accordingly, gas phase reactions stemming off from the initial adduct formation do not become significant until further downstream. Therefore, in this case, showerhead deposition will not occur until about the fifth hole ring junction. Furthermore, a smaller fraction of the total inlet TMG will deposit as more of the adduct has an opportunity to exit the showerhead.

On the other hand, raising the susceptor temperature will have the opposite effect on showerhead deposition. An increase in susceptor temperature causes the gas temperature profile within the showerhead to increase. Adduct dissociation and methane elimination begin to occur much earlier causing deposition to occur closer to the showerhead center.

4. Concluding remarks

In this paper, a detailed deposition chemistry model was developed and applied to a GaN MOVPE reactor showerhead system. A physically based model describing heat transfer and gas transport through the showerhead was previously developed and used in conjunction with this deposition model to study the interplay between the transport of reactants, adduct formation chemistry, and deposition kinetics within a MOVPE reactor showerhead system. The model predictions are in good agreement with

experimental data with minimal parameter fitting with respect to the thermal model. No adjustable parameters were used in the kinetic model. Spatial distributions of deposition patterns predicted from the model are reproduced by experiments. Furthermore, quantitative validation of the model to showerhead weight experiments also demonstrates good agreement. This study has provided further insight into the physical and chemical mechanisms underlying gallium nitride epitaxial film growth.

Acknowledgments

The authors acknowledge the close research collaboration and financial support from the Northrop Grumman Corporation.

References

- [1] C. Theodoropoulos, T.J. Mountziaris, H.K. Moffat, J. Han, *J. Crystal Growth* 217 (2001) 65.
- [2] M.J. Almond, C.E. Jenkins, D.A. Rice, K. Hagen, *J. Organomet. Chem.* 439 (1992) 251.
- [3] D. Mazzaresse, A. Tripathi, W.C. Conner, K.A. Jones, L. Calderon, W. Eckart, *J. Electron. Mater.* 18 (1989) 369.
- [4] R.P. Pawlowski, C. Theodoropoulos, A.G. Salinger, T.J. Mountziaris, H.K. Moffat, J.N. Shadid, E.J. Thrush, *J. Crystal Growth* 221 (2000) 622.
- [5] S.A. Safvi, J.M. Redwing, M.A. Tischler, T.F. Kuech, *J. Electrochem. Soc.* 144 (1997) 1789.
- [6] T.G. Mihopoulos, Ph.D. Thesis, Chemical Engineering Department, Massachusetts Institute of Technology, 1999.
- [7] J. Sun, J.M. Redwing, T.F. Kuech, *Phys. Status Solidi (a)* 176 (1999) 693.
- [8] J. Sun, J.M. Redwing, T.F. Kuech, *J. Electron. Mater.* 29 (2000) 2.
- [9] R.P. Parikh, R.A. Adomaitis, *J. Crystal Growth*, 2005, in press.
- [10] C. Itle, A.G. Slainger, R.P. Pawlowski, J.N. Shadid, L.T. Biegler, *Comp. Chem. Eng.* 28 (2004) 291.
- [11] E. Mesic, M. Mukinovic, G. Brenner, *Comput. Mater. Sci.* 31 (2004) 42.
- [12] K. Harafuji, Y. Hasegawa, A. Ishibashi, A. Tsujimura, I. Kidoguchi, Y. Ban, K. Ohnaka, *Jpn. J. Appl. Phys.* 39 (2000) 6180.
- [13] D.B. Hash, T. Mihopoulos, T.R. Govindan, M. Meyyappan, *J. Vac. Sci. Technol. B* 18 (2000) 2808.
- [14] B.D. Hoffman, R.A. Adomaitis, *IEEE*, 2005, submitted for publication.
- [15] A. Acrivos, B.D. Babcock, R.L. Pigford, *Chem. Eng. Sci.* 10 (1959) 112.
- [16] P.W. Atkins, *Physical Chemistry*, seventh ed., W.H. Freeman, New York, 2002.
- [17] T.J. Mountziaris, S. Kalyanasundaram, N.K. Ingle, *J. Crystal Growth* 131 (1993) 283.
- [18] R.C. Reid, J.M. Prausnitz, B.E. Poling, *The Properties of Gas and Liquid*, McGraw-Hill, New York, 1987.
- [19] M.G. Jacko, S.J.W. Price, *Can. J. Chem.* 41 (1962) 1560.
- [20] R.A. Adomaitis, *Comput. Chem. Eng.* 26 (2002) 981.
- [21] The Mathworks, Inc., (<http://www.mathworks.com>).